Supporting Information for "Electron transport in nanocrystal solids"

(Dated: October 29, 2020)

Contents

I. ATOMISTIC MODEL AND DENSITY-FUNCTIONAL THEORY CALCULATIONS

We used density-functional theory (DFT) with projector-augmented-wave (PAW) potentials,[1] as implemented in VASP,[2] first to determine the equilibrium structure of CdSe nanoplatelets passivated by carboxylate ligands and then to obtain the wavefunctions $\psi(\mathbf{r})$ for the electron and hole quantum-confined states discussed in the main text. The structural calculations were performed within the generalized-gradient approximation of Perdew, Burke, and Ernzerhof (PBE) to DFT,[3] while the wavefunctions were computed using the hybrid screened-exchange functional of Heyd, Scuseria, and Ernzerhof (HSE).[4] For the HSE calculations we used a fraction $\alpha = 0.30$ of Hartree-Fock exchange to accurately reproduce the bulk band gap of zinc-blende CdSe at room temperature.

CdSe nanoplatelets grown from colloidal solution have the zinc-blende crystal structure and exhibit Cd-terminated outer layers [5] and hence we assumed these findings in all our calculations. Since the surface Cd atoms carry a positive charge, it is natural to expect the ligands to bind to these Cd atoms as carboxylate anions. We confirmed this expectation using DFT total energy calculations. We tested several different possible coordinating geometries of the ligand at the nanoplatelet surface. The most stable is the one shown in Fig. 2 of the main text, a mixed bridging-chelating coordination in which the two oxygen atoms of the carboxylate head group form bonds to two surface Cd atoms. Full structural relaxation was performed on the ligand molecules, which we assumed to have 1×1 periodicity (one ligand per surface Cd atom) on both sides of the CdSe nanoplatelet. For simplicity, the platelet itself was kept in its ideal structure because the atomic relaxations from this idealized geometry were found to be negligible. The relaxations were performed in a repeated slab geometry with a vacuum region of 20 Å. The Brillouin-zone sampling was $2 \times 2 \times 1$.

The electron and hole quantum-confined wavefunctions $\psi(\mathbf{r})$ were computed at the Brillouin-zone center using HSE and identified by examining their spatial envelope structure (which for the lowest-lying confined states must be nodeless) and atomic orbital composition (Se(p) for hole states and mixed Cd(s) plus Se(p) for electron states). For our purposes, the wavefunction tails must be represented very accurately. Plane-wave basis sets with standard cutoff energies fail to do this. To ensure the wavefunctions are fully converged, we doubled the default energy cutoff to 800 eV.

The electron and hole quantum-confined wavefunctions $\psi(\mathbf{r})$ were computed at the Brillouin-zone center using HSE and identified by examining their spatial envelope structure and atomic orbital composition. For our purposes, the wavefunction tails must be represented very accurately. Plane-wave basis sets with standard cutoff energies fail to do this. To ensure the wavefunctions are fully converged, we doubled the default energy cutoff to 800 eV.

II. SQUARE-WELL MODEL AND EFFECTIVE-MASS THEORY

A major step in our work was to use a one-dimensional stepped-square-well model and effective-mass theory to reproduce the DFT/HSE wavefunctions as accurately as possible. In this section we describe the details of this procedure. We begin with a brief overview and then give technical details in the following subsections.

The full DFT/HSE wavefunctions $\psi(\mathbf{r})$ are functions of $\mathbf{r} = (x, y, z)$ and so we first performed a planar averaging parallel to the surface plane to define a real-valued one-dimensional wavefunction,

$$\psi(x) = \left[\int |\psi(x, y, z)|^2 dy\, dz \right]^{1/2}, \tag{1}$$

one example of which is shown in Fig. 3(a) of the main text. We then constructed the stepped-square-well potential shown in that figure and solved for its lowest-lying bound state numerically using the transfer-matrix approach described in Sec. II A below. Specifically, we fixed the physical dimensions a and L of the square well and then used effective-mass theory (EMT) to obtain the wavefunctions $\phi_{UV}(x)$, which depend on the square-well barriers U and V. Finally, we performed a two-dimensional numerical optimization with respect to U and V of the objective function

$$\mathcal{E} = \int |\ln \psi(x) - \ln \phi_{UV}(x)|^2 dx \tag{2}$$

to obtain the optimal barrier heights U_0,V_0 and the corresponding optimal wavefunction $\phi(x) = \phi_{U_0 V_0}(x)$ discussed and shown in Fig. 3(a) of the main text.

A. Wavefunctions of a stepped square well

We determined the bound-state wavefunctions for the stepped square well using a transfer-matrix approach developed for one-dimensional heterostructure profiles.[5] We take the potential W_j to be constant in each region

$j = 0, 1, \ldots, N$. The wavefunction in region j has the form

$$\phi_j(x) = A_j e^{-\alpha_j(x-x_j)} + B_j e^{\alpha_j(x-x_j)}, \tag{3}$$

where the wavenumber is $\alpha_j = [2m_j(W_j - E)]^{1/2}/\hbar$, E is the eigenenergy, and m_j is the effective mass. We consider only bound states $E < W_j$. We apply conventional boundary conditions by matching the wavefunctions $\phi_j(x)$ and derivatives $\partial\phi_j(x)/m_j\partial x$ at the boundaries. This leads to a coupled recursion relation for the coefficients A_j and B_j:

$$\begin{aligned} A_j + B_j &= A_{j+1}e^{-\alpha_{j+1}(x_j - x_{j+1})} + B_{j+1}e^{\alpha_{j+1}(x_j - x_{j+1})} \\ \frac{\alpha_j}{m_j}(A_j - B_j) &= \frac{\alpha_{j+1}}{m_{j+1}}[A_{j+1}e^{-\alpha_{j+1}(x_j - x_{j+1})} - B_{j+1}e^{\alpha_{j+1}(x_j - x_{j+1})}]. \end{aligned} \tag{4}$$

This can be written more compactly as

$$\begin{bmatrix} A_{j+1} \\ B_{j+1} \end{bmatrix} = F_{j+1,j} \begin{bmatrix} A_j \\ B_j \end{bmatrix}, \tag{5}$$

where the transfer matrix is

$$F_{j+1,j} = \frac{1}{2}\begin{bmatrix} (1+P_{j+1,j})e^{-\alpha_{j+1}\delta x_j} & (1-P_{j+1,j})e^{-\alpha_{j+1}\delta x_j} \\ (1-P_{j+1,j})e^{\alpha_{j+1}\delta x_j} & (1+P_{j+1,j})e^{\alpha_{j+1}\delta x_j} \end{bmatrix}. \tag{6}$$

For convenience we have defined

$$P_{j+1,j} = \frac{m_j\alpha_{j+1}}{m_{j+1}\alpha_j} \tag{7}$$

and we denote the thickness of region $j+1$ by $\delta x_j = x_{j+1} - x_j$.

To apply the method, we take the leftmost region to be $j = 0$. To ensure the wavefunction is bounded, we must have $A_0 = 0$. Similarly, the wavefunction in the rightmost region must have $B_{N+1} = 0$. The matrix product $f = F_{N+1,N}F_{N,N-1}\cdots F_0$ connects the coefficients:

$$\begin{bmatrix} A_{N+1} \\ 0 \end{bmatrix} = \begin{bmatrix} f_{11} & f_{12} \\ f_{21} & f_{22} \end{bmatrix} \begin{bmatrix} 0 \\ B_0 \end{bmatrix}, \tag{8}$$

In order for this equation to be satisfied, we must have $f_{22}(E) = 0$. The smallest E satisfying this equation is the energy of the ground state.

We now apply this technique to our problem, the symmetric stepped square well. There are three regions: the semi-infinite vacuum with potential V, the ligand region with width L and potential U, and the quantum-well region with width a and potential zero. This leads to

$$\begin{aligned} f_{22}(E) = {} & \cosh^2(\alpha_{\rm lig}L)\Big[2\cos(ka) + \frac{J^2-1}{J}\sin(ka)\Big] \\ & + \sinh^2(\alpha_{\rm lig}L)\Big[2\cos(ka) + \frac{K^2-1}{K}\sin(ka)\Big] \\ & + \sinh(2\alpha_{\rm lig}L)\Big[\frac{M^2+1}{M}\cos(ka) + \frac{N^2-1}{N}\sin(ka)\Big], \end{aligned} \tag{9}$$

where we have defined

$$J = \frac{m_{\rm QW}\alpha_{\rm vac}}{m_{\rm vac}k}, \qquad K = \frac{\alpha_{\rm lig}^2}{m_{\rm lig}^2}\frac{m_{\rm vac}m_{\rm QW}}{\alpha_{\rm vac}k}, \qquad M = \frac{m_{\rm lig}\alpha_{\rm vac}}{m_{\rm vac}\alpha_{\rm lig}}, \qquad N = \frac{m_{\rm QW}\alpha_{\rm lig}}{m_{\rm lig}k} \tag{10}$$

and the wavenumbers in the three regions are given by $k = (2m_{\rm QW}E)^{1/2}/\hbar$, $\alpha_{\rm lig} = [2m_{\rm lig}(U-E)]^{1/2}/\hbar$, $\alpha_{\rm vac} = [2m_{\rm vac}(V-E)]^{1/2}/\hbar$. There are four nonzero wavefunction coefficients: $B_{\rm vac}$, $A_{\rm lig}$, $B_{\rm lig}$, $B_{\rm QW}$. By applying the boundary conditions, we obtain three relationships among them:

$$\begin{aligned} A_{\rm lig} &= \frac{B_{\rm vac}(m_{\rm vac}\alpha_{\rm lig} - m_{\rm lig}\alpha_{\rm vac})}{2m_{\rm vac}\alpha_{\rm lig}}e^{-(\alpha_{\rm vac}+\alpha_{\rm lig})(a/2+L)}, \\ B_{\rm lig} &= \frac{B_{\rm vac}(m_{\rm vac}\alpha_{\rm lig} + m_{\rm lig}\alpha_{\rm vac})}{2m_{\rm vac}\alpha_{\rm lig}}e^{-(\alpha_{\rm vac}-\alpha_{\rm lig})(a/2+L)}, \\ B_{\rm QW} &= \frac{(B_{\rm lig} - A_{\rm lig}e^{\alpha_{\rm lig}a})m_{\rm QW}\alpha_{\rm lig}}{m_{\rm lig}k}e^{-(\alpha_{\rm lig}a)/2}\csc(ka/2). \end{aligned} \tag{11}$$

Requiring the wavefunction to be normalized provides the fourth relationship, and hence the full wavefunction for the stepped square well.

It is worthwhile to check that without the ligand region, our result reduces to the standard solution for a simple (i.e. non-stepped) square well. To see this, we first set $L = 0$ to obtain

$$f_{22}(E) = 2\cos(ka) + \frac{J^2 - 1}{J}\sin(ka) = 0. \tag{12}$$

Using the trigonometric identity $\tan(ka) = 2\tan(ka/2)/[1 - \tan^2(ka/2)]$ we then obtain

$$J = \tan(ka/2), \tag{13}$$

which gives the standard equation for the energy level in a simple quantum well:

$$\alpha_{\rm vac} = k(m_{\rm vac}/m_{\rm QW})\tan(ka/2). \tag{14}$$

Finally, it is easy to confirm that the limit $V \to \infty$ leads to the standard result for the lowest bound-state energy of the infinite potential well,

$$E_0 = \frac{\hbar^2\pi^2}{2m_{\rm QW}a^2}. \tag{15}$$

B. Effective masses of CdSe and ligands

The effective masses $m_{\rm QW}$ (for the CdSe quantum well) and $m_{\rm lig}$ (for the ligand region) are central parameters in the effective-mass-theory solution of the square-well wavefunctions. We used CdSe effective masses obtained from the multiband effective-mass approximation proposed by Pidgeon and Brown[6] and applied recently to zinc-blende CdSe nanoplatelets, $0.893m_e$ (for holes) and $0.183m_e$ (for electrons), where m_e is the electron rest mass.[7] This model correctly describes the non-parabolic behavior of the hole and the electron-band dispersions near the Brillouin-zone center. We used the mass for heavy holes because they determine the energy levels in the CdSe quantum-well region.

We used DFT to calculate a single effective mass for the ligand region by considering a fictitious "alkane solid" consisting of parallel infinite saturated hydrocarbon chains having a lattice spacing given by the surface lattice constant of CdSe(001). We took the effective mass of the light holes because they determine the asymptotic behavior of the wavefunction $\phi(x)$ in the ligand region. The value obtained, $0.287m_e$, is in excellent agreement with the value reported earlier for alkane chains.[8] The corresponding effective mass for electrons is $1.784m_e$.

We must also take into account the effect of the ligand packing density which can, in principle, vary according to the colloidal synthesis, growth temperature, or the use of multiple ligands. At the maximum possible density of one ligand per surface Cd atom, the ligands are separated by 4 Å and interact very little. Hence it is reasonable to spatially average the computed effective masses according to how much of this volume is vacuum-like compared to ligand-like. We explored several ad-hoc definitions for this partitioning and found a reasonable value of $f_{\rm vac} = 0.68$ for the fraction of vacuum-like volume. In this way we arrived at final values for the effective masses of $0.768m_e$ and $1.255m_e$ for light-holes and electrons, respectively.

III. WAVEFUNCTION OVERLAP

A. DFT overlap integrals for electron states

The theoretical values shown in Fig. 4 of the main text of the overlap integral are for hole states. Figure S1 on the following page shows the corresponding values for electron states and the numerically determined decay length L_0.

B. Derivation of analytic expression for the overlap integral

The wavefunction $\phi(x)$ for the stepped square well has the form shown in Eq. 3 with coefficients given by Eq. 11. In the ligand region, this wavefunction is a sum of two exponentials, but their coefficients differ by about six orders of magnitude, $A_{\rm lig} \ll B_{\rm lig}$. Hence, it is an excellent approximation to regard $\phi(x)$ as consisting of $\cos(kx)$

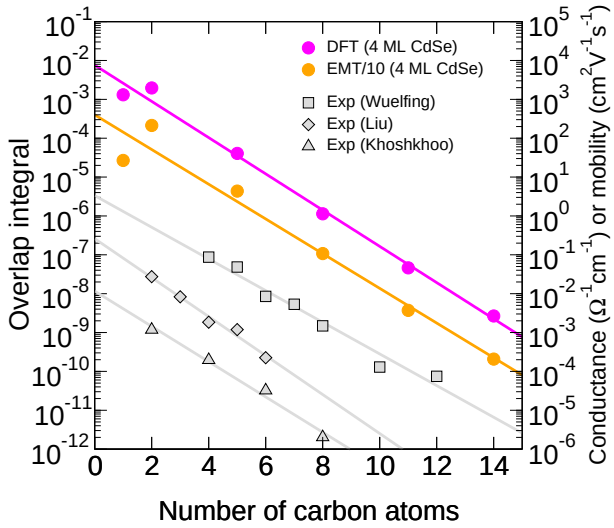

FIG. S1: Overlap integrals from density-functional-theory (DFT) and effective-mass theory (EMT) of the quantum-confined electron-state wave functions for CdSe nanoplatelets as a function of the number of carbon atoms in the ligand molecules. The results for 4-ML platelets obtained from DFT (magenta) and EMT (orange) are in extremely good agreement; the EMT values are offset by one decade for clarity. The exponential decay lengths L_0 are 1.16 Å for DFT and 1.21 Å for EMT. The experimental results (Refs. 9, 10,11) are identical to those in Fig. 4 of the main text.

in the nanoplatelet region and single exponentials $\exp(-\alpha_{\rm lig}|x|)$ and $\exp(-\alpha_{\rm vac}|x|)$ in the ligand and vacuum region, respectively.

We now consider the overlap integral of the normalized wavefunction $\phi(x)$,

$$S(D) = \int \phi(x)\phi(x-D)dx \tag{16}$$

for the case $D = a + 2L + g$ considered in the main text and for simplicity set $g = 0$. This integral can be performed analytically to give

$$\begin{aligned} S(D) = &\Big[2\alpha_{\rm lig}\cos(ak/2)\, e^{-a\alpha_{\rm vac}-2L(2\alpha_{\rm lig}+\alpha_{\rm vac})} \times \\ &\Big[\cos(ak/2)\left(-2\alpha_{\rm vac}(\alpha_{\rm lig}+\alpha_{\rm vac})\left(\alpha_{\rm vac}^2+k^2\right)e^{a\alpha_{\rm vac}+2L(\alpha_{\rm lig}+\alpha_{\rm vac})}\right. \\ &+ 2\alpha_{\rm vac}(\alpha_{\rm lig}+\alpha_{\rm vac})\left(\alpha_{\rm lig}\alpha_{\rm vac}+k^2\right)e^{\alpha_{\rm vac}(a+L)+3\alpha_{\rm lig}L} \\ &+ (\alpha_{\rm lig}-\alpha_{\rm vac})^2\left(\alpha_{\rm vac}^2+k^2\right)e^{2\alpha_{\rm lig}L} - 2\alpha_{\rm vac}(\alpha_{\rm lig}-\alpha_{\rm vac})\left(\alpha_{\rm lig}\alpha_{\rm vac}-k^2\right)e^{L(3\alpha_{\rm lig}+\alpha_{\rm vac})}\Big) \\ &+ 2\alpha_{\rm vac}k\left(e^{a\alpha_{\rm vac}}+1\right)(\alpha_{\rm lig}-\alpha_{\rm vac})(\alpha_{\rm lig}+\alpha_{\rm vac})\sin(ak/2)\, e^{L(3\alpha_{\rm lig}+\alpha_{\rm vac})}\Big]\Big] \\ &/\Big[\alpha_{\rm vac}(\alpha_{\rm lig}-\alpha_{\rm vac})(\alpha_{\rm lig}+\alpha_{\rm vac})\left(\alpha_{\rm vac}^2+k^2\right)\times \\ &\left(a\alpha_{\rm lig}+\frac{\alpha_{\rm lig}\sin(ak)}{k}+\frac{(\alpha_{\rm lig}-\alpha_{\rm vac})e^{-2\alpha_{\rm lig}L}(\cos(ak)+1)}{\alpha_{\rm vac}}+\cos(ak)+1\right)\Big]. \end{aligned} \tag{17}$$

Evaluating this expression using realistic parameters and then dropping numerically negligible terms (those at least three orders of magnitude smaller than other terms) leads to

$$S(D) = \frac{2\alpha_{\rm lig}\cos\left(\frac{ak}{2}\right)e^{-a\alpha_{\rm vac}-2L(2\alpha_{\rm lig}+\alpha_{\rm vac})}\left(\cos\left(\frac{ak}{2}\right)\left(-2\alpha_{\rm vac}(\alpha_{\rm lig}+\alpha_{\rm vac})\left(\alpha_{\rm vac}^2+k^2\right)e^{a\alpha_{\rm vac}+2L(\alpha_{\rm lig}+\alpha_{\rm vac})}\right)\right)}{\alpha_{\rm vac}(\alpha_{\rm lig}-\alpha_{\rm vac})(\alpha_{\rm lig}+\alpha_{\rm vac})\left(\alpha_{\rm vac}^2+k^2\right)\left(a\alpha_{\rm lig}+\frac{\alpha_{\rm lig}\sin(ak)}{k}+\cos(ak)+1\right)} \tag{18}$$

which can be rearranged to

$$S(D) = \exp(-L/L_0)\xi(a), \tag{19}$$

where $L_0 = 1/2\alpha_{\rm lig}$ and we have defined a function that expresses the size dependence,

$$\xi(a) = \frac{2\alpha_{\rm lig}k(\cos(ak)+1)}{(\alpha_{\rm vac}-\alpha_{\rm lig})(a\,\alpha_{\rm lig}k + \alpha_{\rm lig}\sin(ak) + k\cos(ak)+k)}, \tag{20}$$

which is independent of L as stated in the main text. For small a we can write a first-order approximation for this,

$$\xi(a) \approx \frac{A_{vl}}{a+2L_0} \tag{21}$$

where $A_{vl} = 2/(\alpha_{\rm vac}-\alpha_{\rm lig})$, as stated in the text.

IV. ANALYTIC BEHAVIOR OF THE DECAY LENGTH

In the previous section, we showed that the decay length describing the exponential dependence of the overlap integral on the ligand length is given by $L_0 = 1/2\alpha_{\rm lig}$, where $\alpha_{\rm lig}$ is the exponent in the wavefunction in the ligand region. In this section, we obtain an expression for $\alpha_{\rm lig}$ that shows why the decay length is primarily determined by the properties of the ligand region and depends only weakly on the nanocrystal size.

It is easy to demonstrate numerically that $\alpha_{\rm lig}$ for the stepped square well is almost independent of the width L of the ligand region. Hence, we consider the limit $L \to \infty$, which is equivalent considering a single (non-stepped) square well.

The standard textbook solution of the single square well is based on effective-mass theory. There are two boundary conditions, ensuring continuity of the wavefunction and its flux. The ratio of the two resulting equations gives the standard square-well equation which we cast in the form of a function,

$$f(E) = m_{\rm QW}\,\alpha_{\rm lig} - m_{\rm lig}\,k\tan ka/2, \tag{22}$$

whose zeroes are the energies of the bound states. Here, $m_{\rm QW}$ and $m_{\rm lig}$ are the effective masses in the quantum well and the ligand region, respectively, $\alpha_{\rm lig} = [2m_{\rm lig}(U-E)]^{1/2}/\hbar$ describes the exponential wavefunction in the ligand region, and $k = (2m_{\rm QW}E)^{1/2}/\hbar$ describes the cosine wavefunction in the quantum well. The function $f(E)$ has a singularity at $E = \hbar^2\pi^2/2m_{\rm QW}a^2$ corresponding to the infinite square well but in our case the zeroes are far from this singularity. Thus we can make a Taylor expansion with respect to E,

$$f(E) \approx \frac{m_{\rm QW}\sqrt{2m_{\rm lig}U}}{\hbar} - \frac{m_{\rm QW}(2am_{\rm lig}\sqrt{U}+\hbar\sqrt{2m_{\rm lig}})}{2\sqrt{U}\hbar^2}E - \frac{4a^3m_{\rm lig}m_{\rm QW}^2U^{3/2}+3m_{\rm QW}\hbar^3\sqrt{2m_{\rm lig}}}{24U^{3/2}\hbar^4}E^2, \tag{23}$$

and use the terms up to 1st order to define a linear approximation to $f(E)$. The zeroes of this linear approximation overestimate the exact energies by 10-20% but since the energy is generally small compared to U this error does not significantly affect $\alpha_{\rm lig}$. Using this linear approximation for E we obtain, after some algebra, the expression for the decay length given in the main text,

$$L_0 = 1/2\alpha_{\rm lig} = \mathcal{L}_0\left[1 - \frac{2}{1+(U/U_0)^{1/2}}\right]^{-1/2}, \tag{24}$$

where

$$\mathcal{L}_0 = \frac{1}{2}\frac{\hbar}{(2m_{\rm lig}U)^{1/2}} \tag{25}$$

is the decay length in the limit of large U and a and we have defined a characteristic energy scale,

$$U_0 = \frac{\hbar^2}{2m_{\rm lig}a^2}. \tag{26}$$

It is evident from these expressions that the nanocrystal size a affects the decay length L_0 only through the term U_0, which is of order a few 10s of meV. This is much smaller than the barrier U, which is of order 1-2 eV. Hence we can write a Taylor expansion of Eq. 24 with respect to $1/a$,

$$L_0 \approx \mathcal{L}_0[1 + 2\mathcal{L}_0/a + 2\mathcal{L}_0^2/a^2]. \tag{27}$$

Since $\mathcal{L}_0$ is of order 1 Å, it is obvious from Eq. 27 that the size dependence of L_0 is very weak.

V. GEOMETRICAL EFFECT OF NANOCRYSTAL SIZE

We model the decay of a wavefunction from the surface of a sphere with radius R into the vacuum using the simple function $f_R(\mathbf{r}) = \exp(-r/L_1)$ for $r > R$ (outside the sphere) and unity inside. Our DFT calculations show that the decay length L_1 is of order 1 Å for decay into vacuum.

Consider now the integral $F(R) = \int f_R(\mathbf{r}) f_R(\mathbf{r} - \mathbf{D}) d^3r$ where, for simplicity, we set the center-to-center separation D such that the spheres are just touching. This integral can be performed analytically but has an extremely complicated form. More illuminating are the two numerical results in Fig. S2 below, which show the dependence of $F(R)$ on R for fixed $L_1 = 1.5$ Å, and on L_1 for fixed $R = 50$ Å. It is obvious from these results that $F(R) \propto RL_1^2$ to within reasonable accuracy, as written in the main text.

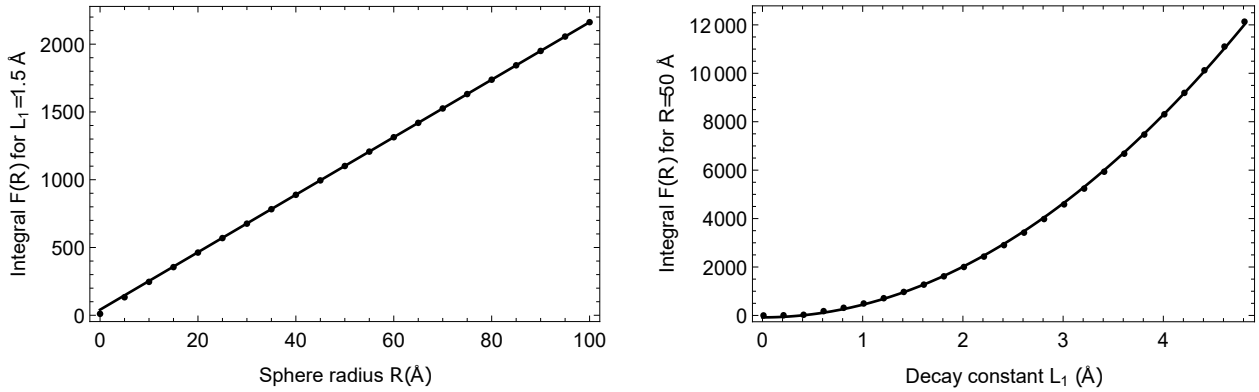

FIG. S2: (left) Linear dependence of $F(R)$ on sphere radius R. (right) Quadratic dependence of $F(R)$ on decay length L_1.

[1] P. E. Blöchl, Physical Review B **50**, 17953 (1994).
[2] G. Kresse and J. Furthmüller, Physical Review B **6**, 15 (1996).
[3] J. P. Perdew, K. Burke, and M. Ernzerhof, Physical Review Letters **77**, 3865 (1996).
[4] J. Heyd, G. E. Scuseria, and M. Ernzerhof, The Journal of Chemical Physics **118**, 8207 (2003).
[5] S. L. Chuang, *Physics of Photonic Devices* (John Wiley and Sons, Inc., New Jersey, 2nd Edition, 2009).
[6] C. R. Pidgeon and R. N. Brown, Physical Review **146**, 575 (1966).
[7] S. Ithurria, M. D. Tessier, B. Mahler, R. P. Lobo, B. Dubertret, and A. L. Efros, Nature Materials **10**, 936 (2011).
[8] J. K. Tomfohr and O. F. Sankey, Physical Review B **65**, 1 (2002).
[9] W. P. Wuelfing, S. J. Green, J. J. Pietron, D. E. Cliffel, and R. W. Murray, Journal of the American Chemical Society **122**, 11465 (2000).
[10] Y. Liu, M. Gibbs, J. Puthussery, S. Gaik, R. Ihly, H. W. Hillhouse, and M. Law, Nano Letters **10**, 1960 (2010).
[11] M. S. Khoshkhoo, J. F. L. Lox, A. Koitzsch, H. Lesny, Y. Joseph, V. Lesnyak, and A. Eychmüller, ACS Applied Electronic Materials **1**, 1560 (2019).